CCC 2018

Proceedings of the Creative Construction Conference (2018)
Edited by: Miroslaw J. Skibniewski & Miklos Hajdu
DOI 10.3311/CCC2018-015

Creative Construction Conference 2018, CCC 2018, 30 June - 3 July 2018, Ljubljana, Slovenia

Volume - forming 3D concrete printing using a variable - diameter square nozzle

Jie Xu*, Lieyun Ding

Hubei Engineering Research Center for Virtual, Safe and Automated Construction,
Department of Construction Management, School of Civil Engineering and Mechanics, Huazhong University of Science and Technology,
No.1037 Luoyu Road, Wuhan 430074, P.R. China

Abstract

3D Concrete Printing (3DCP) process is rapidly developing worldwide, showing its ability to construct large-scale components or even a building. However, the current 3DCP process has found it hard to manufacture architectural components with detailed ornamentations and features on their surface due to the Fused Deposition Modelling (FDM) manner that generates fixed-width thick filaments. This paper introduces a novel Volume - Forming 3D Concrete Printing (VF3DCP) method applying a variable-diameter square nozzle to manufacture architectural ornaments. The VF3DCP method directly fabricates a variable cross-section volume during one-time work instead of an FDM accumulation process. A VF3DCP extrusion kit prototype containing a steering module and a nozzle-varying module and a particular adaptive tool path planning algorithm are developed. Functional relationships of four key process parameters for a trial material, including nozzle diameter, nozzle moving velocity, material extrusion rate and tool path curvature radius, are fitted by process tests. Finally, a case study into a VF3DCP architectural carve pattern is conducted, which shows the potential of the proposed method in manufacturing architectural ornaments.

Peer-review under responsibility of the scientific committee of the Creative Construction Conference 2018.

Keywords: concrete printing; volume forming; variable nozzle; architectural ornament

1. Introduction

3D Concrete Printing (3DCP) processes have been gaining ground since the first process was developed, notably in the mid-1990s in California, USA, when Khoshnevis released a method termed Counter Crafting (CC) [1]. This process was continuous extrusion - deposition of concrete filaments to manufacture a wall structure. Another notable work was published by the team at Loughborough University [2,3], who used a similar process to fabricate large-scale components (i.e. wonder bench, doubly-curved panel). Now there are more than 35 institutes and enterprises participating in this developing area [4-10]. As the most prevalent Additive Construction (AC) method [11], these 3DCP processes are supposed to provide the construction industry with enormous potential benefits (i.e. labor, cost, waste). According to Bos et al. [12], the current 3DCP groups are either production-oriented or performance-oriented; nevertheless, both of them are drawing the public sight into the ability of the 3DCP process to construct large-scale components (e.g. walls, columns) or even buildings (e.g. houses, offices).

Compared to powder-based AC method [13], the 3DCP process that adopts the Fused Deposition Modelling (FDM) principle, usually has lower printing resolution on printed surfaces. This can be termed as a Line - Forming method, that is, the nozzle of a printer deposits material in lines (filaments) and numbers of lines accumulate to obtain a surface and then an entity. Usually, a predefined nozzle diameter is used for an entire Line - Forming process, which inevitably causes the staircase effect - a geometric approximation manner of a curved surface by uniform-thickness layers [14-

Corresponding author: Jie Xu email: xu_jie@hust.edu.cn

16]. Acceptable geometries may be achieved by such 3DCP process for constructing large-scale components if the fixed-width filaments are thin enough. Referring to Loughborough's achievement of 6mm for filament width [17], the limit on the minimal filament width has severely inhibited the 3DCP process from manufacturing architectural ornamental components which typically possess fine and intricate features (e.g. patterns, carvings) on their surface (Fig. 1). When implemented with fixed-width filaments, the 3DCP products are likely to have missing and superfluous parts, or even distortions, which is an inherent deficiency of 3DCP process.

Fig. 1. Façade panel, carved window and decorated bracket with patterns.

To fabricate accurate geometries of architectural ornaments as well as other grotesque functional components, this study attempts to revolutionize the current Line - Forming 3DCP process by a novel Volume - Forming 3D Concrete Printing (VF3DCP) method using a variable - diameter square nozzle. The VF3DCP process aims to provide a conventionally fixed-width filament with distinctly variable cross-sections, transforming the filament from a line into a volume. The VF3DCP method is able to directly fabricate an entity formed by variable cross-section concrete filaments (or lumps) during one-time work instead of line accumulation, which is rather different from the Line - Forming process. This is supposed to produce excellent geometries for components with high-quality outward appearances such as architectural ornaments. A custom VF3DCP extrusion kit prototype is designed to demonstrate the process and a case study of a carve pattern manufacture is undertaken to validate the VF3DCP method.

2. VF3DCP extrusion kit prototype composition and running mode

The patented VF3DCP extrusion kit prototype (Fig. 2) is mounted on a steel lifting beam of a movable gantry. The kit consists of four functional modules, referring to mixing module, depositing module, steering module and nozzle - varying module. The nozzle is designed into a square and the modularized design of the kit makes it easy to disassemble and assembled each module.

- *Mixing module*: this module mainly includes an electric motor, a stirring impeller and a charging spout. The electric motor powers the stirring impeller with an appropriate rotation rate to keep the mobility of the cement mortar fed into the charging spout.

- *Depositing module*: this module mainly contains a servo motor with a reducer, a coupling, a bearing block and a screw conveyer. Driven by the reduced servo motor, the screw conveyer sucks the stirred material in the charging spout and vertically deposits it in a required flow rate.

- *Steering module*: this module mainly incorporates a servo motor with a reducer, a turn-barrel and a locking block. The turn-barrel, besieging the screw conveyer through the locking block, is driven by the servo motor to rotate the square nozzle according to tool paths.

- *Nozzle - varying module*: this module mainly comprises a servo motor with a reducer, a rotary turntable, a spacing plate, four small isosceles - triangle plates with four pairs of sliders and tracks. Powered by the motor, the rotary turntable rotates to make the plates centrifugally or centripetally move to change the nozzle diameter.

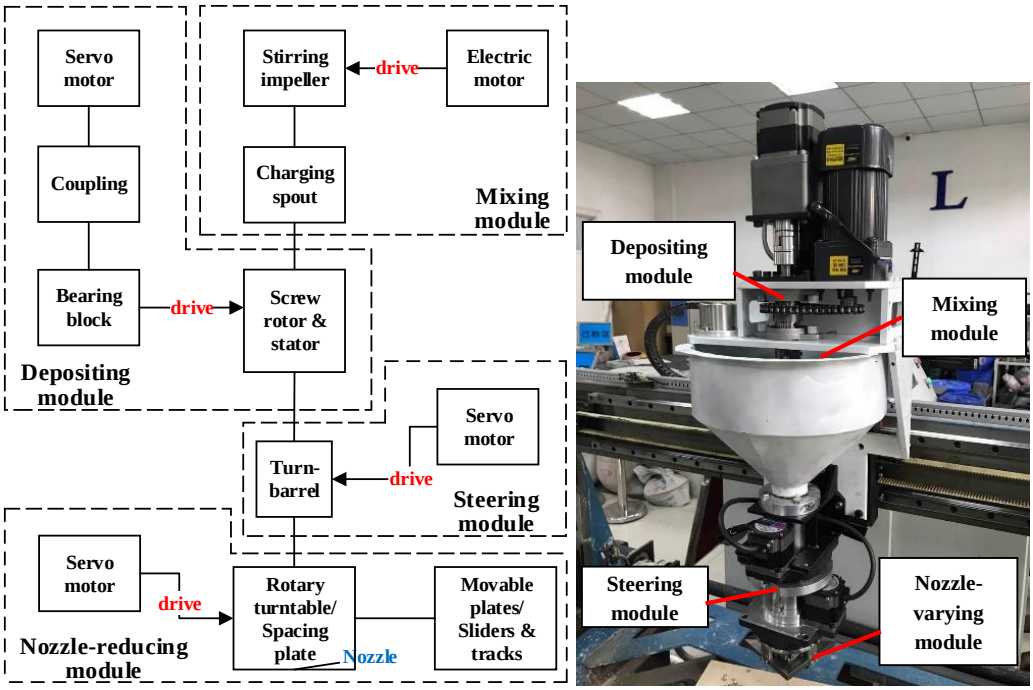

Fig. 2. The VF3DCP extrusion kit prototype composition.

A Volume - Forming process means that the width, height and orientation of any cross-section of a filament should precisely equal to the target geometry, which primarily results from the co-operative running of the nozzle - varying module and the steering module. The four identical isosceles - triangle moveable plates of the nozzle - varying module closely join up with each other in the same horizontal plane, generating a centrosymmetric structure. Every plate gains a rigid connection with a slider that links with a turntable via a bearing. When a rotating signal is received, the servo motor will drive the turntable to rotate relatively to the turn-barrel of the steering module, causing the four sliders to simultaneously slither along their tracks upon a board fixed on the turn-barrel. Then, the four isosceles - triangle plates are forced to move centrifugally or centripetally, which brings about displacements along interfaces of these plates to obtain a variable - diameter square nozzle. Notably, the square nozzle is able to change its diameter from 0mm to 25mm while its center keeps constant (Fig. 3). The steering module is in charge of driving the moving nozzle to rotate. When a rotation signal is received, the turn-barrel will be rotating synchronously with the revolving part of a servo motor, which finally causes the nozzle rotation. This ensures two opposite edges of the square nozzle to be constantly parallel to tool paths, achieving excellent surface perpendicularity of deposited filaments. Therefore, the coordinated running of both the nozzle - varying module and the steering module makes it possible for the extrusion kit to manufacture a complex geometry volume.

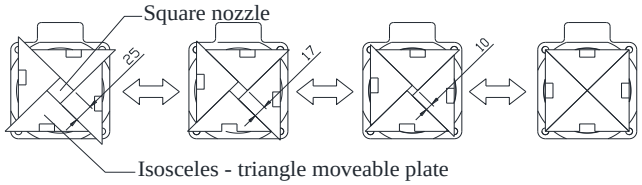

Fig. 3. The variable - diameter square nozzle for the VF3DCP process.

3. Process tests for functional relationships fitting of key process parameters

To realize a VF3DCP process, functional relationships of process parameters need to be set up to run the machine with a particular material. Generally, the key process parameters include the nozzle diameter, the nozzle moving

velocity, the material extrusion rate and the tool path curvature radius. However, these parameters can critically vary from different material composition applied for manufacture. To demonstrate the VF3DCP process, a feasible material composition is proposed (Table 1). The P.C32.5R Composite Portland cement is used while the natural river sand is screened at 1.2 mm. A 30s dry mixing of cellulose ether, cement and sand is taken, followed by another 3min wet mixing. With this trial material, functional relationships of the key process parameters are respectively fitted by experimental matched values of these parameters from two process tests (room temperature) on the stipulation that both width and height of any cross-section of a filament always equal to the nozzle diameter. Test I is to determine the functional relationship among the nozzle diameter, the nozzle moving velocity and the material extrusion rate; test II is for the functional relationship between the tool path curvature radius and the nozzle moving velocity.

Table 1. Trial material composition.

Item	Water-cement ratio	Sand-cement ratio	Water reducer addition amount (relative to cement)	Cellulose ether addition amount (relative to cement)
Value	0.35	1:1	0.1%	0.05%

3.1. Process test I

In this test, four nozzle diameters of 10mm, 15mm, 20mm and 24mm (25mm is discarded for that the nozzle would easily get stuck) are respectively used to deposit four groups of straight filaments in length of approx. 20cm. Each group has ten filaments with different nozzle moving velocities varying from 10mm/s to 100mm/s (gradient value of 10mm/s) and different suitable material extrusion rates. By naked - eye observation with ruler measurements on three interquartile positions of a filament, each filament has to be checked on the geometry conformity between its cross-section and the nozzle. Usually, a number of different extrusion rates are tried to fit in with a certain nozzle moving velocity for a set nozzle diameter before a suitable extrusion rate is recorded manually. The satisfactory filaments are presented in Fig. 4 with gradually increased nozzle moving velocities from the top to the bottom for each group. However, there can be measurement errors of 1-2mm deviations for the filament cross-sections. The first five and the next five filaments in the group of 10mm nozzle are deposited in two different places (Fig. 4a). The material gets a bit drier after an open time of approx.90min when filaments of 20mm nozzle diameter are deposited, resulting in some surface cracks and the last filament of 100mm/s nozzle moving velocity is left out due to a material shortage (Fig. 4c). The last group of filaments is deposited using newly mixed material (Fig. 4d). Notably, filaments of the second group, the 15mm nozzle diameter, have the most excellent printed surfaces.

a b c d

Fig. 4. Four groups of deposited filaments in different set nozzle diameter, (a) 10mm; (b) 15mm; (c) 20mm; (d) 24mm.

The experimental matched values of the three process parameters are recorded in Table 2. The material extrusion rate increases along with the nozzle moving velocity in each group; however, it just fluctuates at first with the nozzle diameter rises and then goes up when the nozzle diameter exceeds 15mm. This implies that the rheology of material being deposited can change significantly when the nozzle diameter decreases to some extent, which makes it harder or even impossible for an undersized nozzle to extrude material. Values in Table 2 are inputted into *MATLAB* for fitting process. The nozzle diameter, the nozzle moving velocity and the material extrusion rate are severally denoted as x, y and z. The fitted function $z = f(x, y)$ is shown in Appendix A.

Table 2. Experimental matched values of the nozzle diameter, the nozzle moving velocity and the material extrusion rate.

Nozzle diameter (mm)	10	10	10	10	10	10	10	10	10	10
Nozzle moving velocity (mm/s)	10	20	30	40	50	60	70	80	90	100
Material extrusion rate (r/s)	0.4	0.5	0.6	0.7	0.8	1.0	1.2	1.5	1.8	2.2
Nozzle diameter (mm)	15	15	15	15	15	15	15	15	15	15
Nozzle moving velocity (mm/s)	10	20	30	40	50	60	70	80	90	100
Material extrusion rate (r/s)	0.2	0.4	0.6	0.8	1.0	1.2	1.4	1.6	1.8	2
Nozzle diameter (mm)	20	20	20	20	20	20	20	20	20	—
Nozzle moving velocity (mm/s)	10	20	30	40	50	60	70	80	90	—
Material extrusion rate (r/s)	0.4	0.6	0.9	1.2	1.4	1.6	1.9	2.3	2.8	—
Nozzle diameter (mm)	24	24	24	24	24	24	24	24	24	24
Nozzle moving velocity (mm/s)	10	20	30	40	50	60	70	80	90	100
Material extrusion rate (r/s)	0.5	0.8	1.2	1.6	2.2	3.0	3.8	4.6	5.5	6.4

Note: The material extrusion rate is represented by the servo motor rotation rate of the depositing module of the VF3DCP extrusion kit.

3.2. Process test II

When a nozzle moves too fast along a tool path of a rather small curvature radius, torsion is very likely to occur in a filament. So, suitable nozzle moving velocities have to be applied to different tool path curvature radiuses, which depends on the functional relationship between the two key process parameters, fitted in this process test. A selected set of eleven one - fourth arc filaments with different curvature radiuses (40mm, 50mm, 100mm, 150mm, 200mm, 250mm, 300mm, 350mm, 400mm, 450mm, 500mm) is deposited using the 15mm nozzle diameter (the best working nozzle diameter in process test Ⅰ). The geometry conformity between the cross-sections of a filament and the nozzle is also manually checked by ruler measurements. The satisfactory arc filaments are presented in Fig. 5.

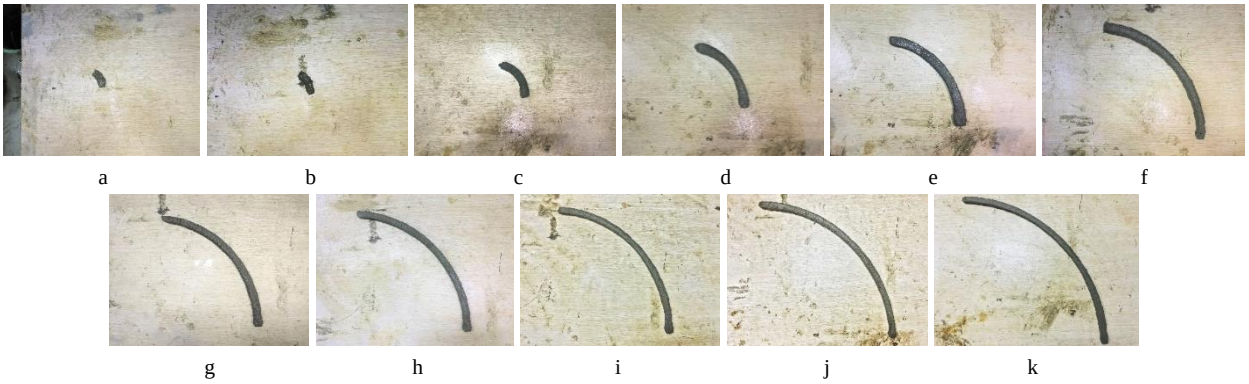

Fig. 5. Eleven one - fourth arc filaments deposited with different curvature radius, (a) 40mm; (b) 50mm; (c) 100mm; (d) 150mm; (e) 200mm; (f) 250mm; (g) 300mm; (h) 350mm; (i) 400mm; (j) 450mm; (k) 500mm.

The suitable nozzle moving velocities experimentally matched with the eleven curvature radiuses are recorded in Table 3. The nozzle moving velocities are finalized by most larger values under the premise of no torsions. Values in Table 3 are inputted into *MATLAB* to fit the functional relationship of the nozzle moving velocity and the tool path curvature radius, which are respectively denoted as y and r. The fitted function $y = g(r)$ is shown in Appendix B.

Table 3. Experimental matched values of the nozzle moving velocity and the tool path curvature radius.

Tool path curvature radius (mm)	40	50	100	150	200	250	300	350	400	450
Nozzle moving velocity (mm/s)	20	25	30	36	43	50	58	67	77	88

Combing the above two fitted functions, the functional relationship of *x*, *y*, *z* and *r* can be figured out as

$$z = f(x,\ y) = f[x,\ g(r)] \tag{1}$$

where *x* and *r* are dependent on the target geometry to be fabricated. However, Eq. (1) applies to the condition that both width and height of filament cross-sections constantly equal to the nozzle diameter, in which case the layer thickness will be variable within one layer due to variable nozzle diameter. To achieve constant layer - thickness manufacture, thinner filaments need to increase their cross-section heights to that of the thickest filament (denoted as *Dmax*) within one layer while their widths remain unchanged. In the light of equal volume principle, the nozzle moving velocity should be adjusted. Supposing the adjusted moving velocity and extrusion rate are *Y* and *Z*, *y* is replaced by *Y* with $y = Y*Dmax / x$ in the function $z = f(x, y)$. Then, we have $Z = F(x, Y)$ with $Y = g(r)$. Therefore, the final functional relationship of the four key process parameters for constant - layer manufacture is

$$Z = F(x,\ Y) = F[x,\ g(r)], Y \in [10, 100] \tag{2}$$

In Eq. (2), *Y* is valued as *10* if $Y<10$ and valued as *100* if $Y>100$. Other process parameters such as the rotation speeds of the turn-barrel and the rotary turntable are set up with suitable values to well support the VF3DCP process.

4. Case study: An architectural carve pattern

An architectural carve pattern is commonly used as an ornamental window (or door) or as an ornamentation to walls and facades (Fig. 1). It usually embodies a number of variable - width curve stripes in same thickness, which is a 2.5D geometry [19]. In the following, a typical architectural carve pattern is designed (Fig. 6) and fabricated by the VF3DCP method. The width of its inner stripes varies from 9mm to 24mm and that of its contour is 18mm.

4.1. Tool path generation

The VF3DCP adopts an adaptive tool path planning approach. The geometry of every curve stripe is calculated by a VF3DCP program to generate the stripe skeleton lines (central lines) as tool paths (with specific curvature radiuses) and also capture the variable widths of each stripe and the contour to determine the nozzle diameters. With the nozzle moving velocity and material extrusion rate figured out by Eq. (2), the nozzle is supposed to move along all the curve stripes and the contour in appropriate velocities with its changing diameter constantly equal to the widths of stripes and contour. The tool paths generating solution procedures are presented as follows.

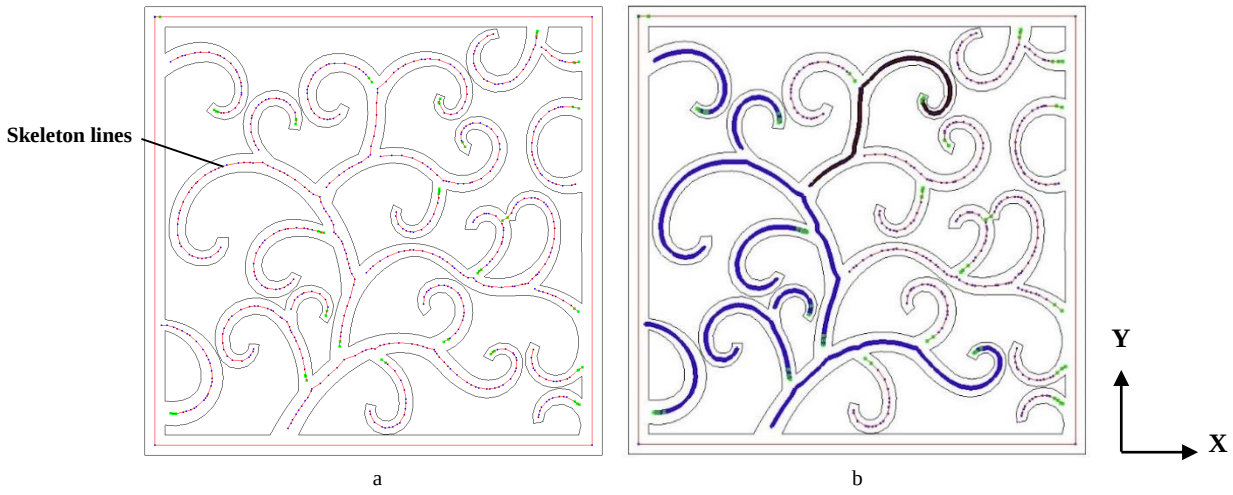

Fig. 6. (a) A designed architectural carve pattern with complete skeleton lines; (b) Tool paths planning (black stripe: current tool path being planned; blue stripes: tool paths that have been planned).

- *Step 1 - Initial skeleton lines generation*: A classical *Voronoi Diagram* algorithm [18] is first applied to the carve pattern, generating a number of the skeleton line-segments (red lines in Fig. 6a) with their pairs of endpoints (blue points in Fig. 6a) for all the inner stripes and the contour. A filtering treatment is done to discard those wrong line-segments outside of the stripe graphic entities, leaving all the correct line-segments connected to obtain the initial skeleton lines for this pattern. There are three types of endpoints in the initial skeleton lines - edge points, normal points and branch points, which respectively have one, two and three line-segments connected (Fig. 7).

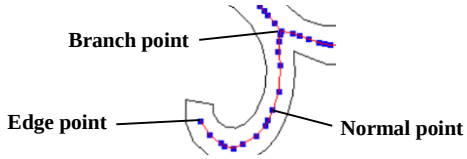

Fig. 7. Three types of endpoints in the skeleton lines.

- *Step 2 - Complete skeleton lines generation*: The initial skeleton lines need to be refined to reach final complete skeleton lines. For any two joint stripes (or contour), redundant skeleton line-segments that cause excessive material deposition at the branch point need to be removed. As shown in Fig. 8a, there are three successive line-segments along each branch from the branch point P_B with an end point (P_{N1}, P_{N2} and P_{N3}, respectively). In the pair of branch P_B P_{N1} and P_B P_{N2}, distances from the four intermediate normal points and point P_B to line P_{N1} P_{N2}, are represented by l_1, l_2, l_3, l_4 and l_5. These five distances are calculated and summed for each line, P_{N1} P_{N2}, P_{N1} P_{N2} and P_{N1} P_{N2}. A pair of branches that possesses the smallest summed-distance value would be kept connected at point P_B while the other branch would be pruned off by a certain length at its tail. Then, point P_B is transformed into a normal point (namely b-normal point) and point P_{N2} becomes a new edge point hereafter (Fig. 8b). As for the initially generated square contour, its four vertexes are distinguished by their maximal or minimal x / y coordinates among all the endpoints. These four vertexes would be successively lined to each other to generate a new contour which is much smoother. Therefore, the complete skeleton lines are figured out.

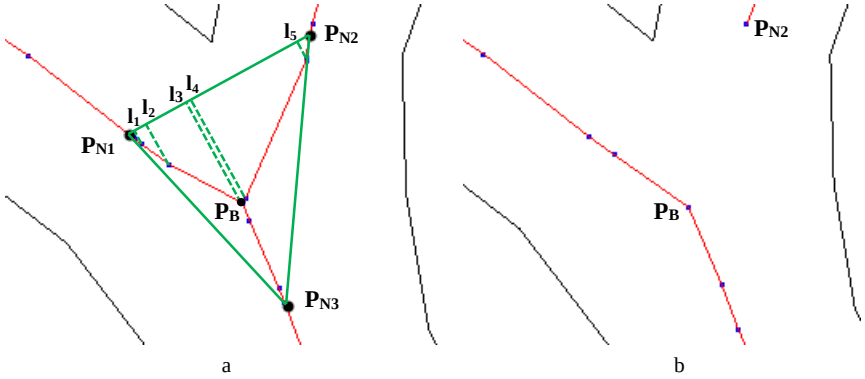

Fig. 8. (a) A branch point of two inner stripes; (b) Pruning of a branch.

- *Step 3 - Tool path planning*: The tool paths are planned along the complete skeleton lines, going from the inner curve stripes to the contour. For the stripes, a tool path is planned by traversal calculation, starting from an edge point that has the minimal x coordinate value among all the endpoints of unplanned paths and travelling through all the normal points (including b-normal points) until another edge point (Fig. 6b). Thus repeatedly, all tool paths can be planned from the area of small x coordinate values to the area of big ones. For the contour, a circle tool path would start from the vertex of minimal x coordinate and maximal y coordinate and also end up with it.

4.2. Pattern printing

The designed 2.5D carve pattern ornament is physically manufactured using the VF3DCP method with the trial material (Fig. 9). The curve stripes are printed before the square contour that encloses the stripes. During the printing

process, two specific geometric features, the corner and the edge point, have been specially treated in that they have a significant impact on the overall print quality.

- *Corner*. A tool path contains a number of included angles (corners) between any two adjacent skeleton line-segments. These corners are separately treated for the inner stripes and the contour. For the inner stripes, the nozzle directly passes a corner from a former line-segment to a latter one while simultaneously rotating a required angle and depositing material. The rotation speed of the turn-barrel is set up as 450° /s, allowing the nozzle to instantly reach the right orientation for the latter line-segment. However, when the nozzle goes through a corner in the square contour, it would stop moving and depositing material but remain at the vertex to finish a rotation of 90° . Then the nozzle re-deposits material 0.1s ahead of re-moving to ensure continuous and ample material deposition.

- *Edge point*. A tool path starts from an edge point and ends up at another one. Given that the material is deposited from the nozzle onto the supporting surface, a time delay of nozzle movement is set up to obtain required material deposition in the beginning. On the other side, when the nozzle comes to a path end, its diameter is reduced to 3mm at a distance of 10mm (seen as green points in Fig. 6b) from the path end, aiming to cut off the filament in advance to obtain a neat end.

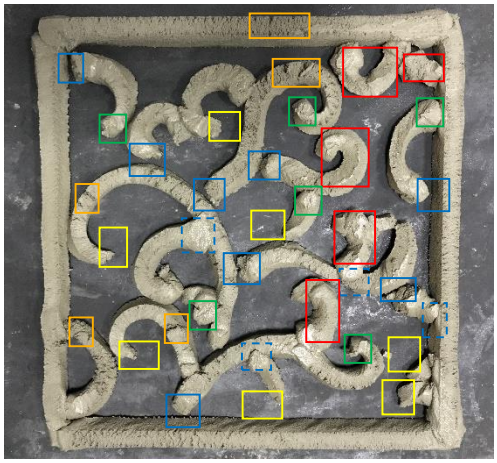

Fig. 9. The manufactured 2.5D pattern ornaments by the VF3DCP method.

Overall, the fabricated VF3DCP pattern looks close to its design (Fig. 6) despite the variable widths of curve stripes may seem somewhat inaccurate due to fitting errors of the functional relationships of the key process parameters. This pattern, however, is hard to manufacture by the conventional 3DCP process using a fixed-width nozzle. Some machine-based manufacture errors remaining to be solved in the future are presented as follows:

- *Accumulated error of included angles*: The current program allows no time for the nozzle to rotate at each corner with a curve stripe, which forces the nozzle to achieve a required rotation in the latter line-segment when it passes a corner. When the nozzle rotation speed is too low to finish the rotation within this line-segment, an error of included angle is generated and delivered to the next corner. Such errors are stripe-by-stripe accumulated from the start to the end, which leads to the skew and torsion of later-deposited stripes, especially those short stripes with high curvatures (red boxes in Fig. 9). Obviously, a higher rotation speed is supposed to alleviate the accumulated error of included angles while the current rotation speed of 450° /s is restrained by the machine capability.

- *Missed deposition at the beginning of a tool path*: The material in the nozzle will be deformed after a filament is cut off at the end of the last tool path. This claims for sufficient time for the nozzle to re-establish a steady state of material extrusion driven by the screw conveyer at the beginning of the current tool path. Inaccurate time delay control of nozzle movement at the start edge points results in missed depositions (yellow boxes in Fig. 9).

- *Deformation at the end of a tool path*: The nozzle can be reduced to no less than approx. 3mm when extruding the trial material for fear of getting stuck. However, this early reduction at the end of a path leads to the concrete

filament being deposited cannot be completely cut off but dragged on a short distance and probably extended and warped a bit at its tail (green boxes in Fig. 9).

- *Disconnection or imperfect connection of two stripes*: Excessive punching of branches may cause some disconnections of two stripes where they are expected to be (blue boxes in Fig. 9). Some other connections of two stripes are unsatisfactory where the joints hardly appear in designated profiles (dashed blue boxes in Fig. 9) since the nozzle cannot change its shape other than square to fit different joint profiles.

- *Surface cracks of stripes*: The material is extruded by a screw conveyer which offers much less pressure compared to a screw pump. So, it is no doubt that there are apparent cracks on the stripe surfaces (orange boxes in Fig. 9).

5. Discussion and conclusions

This study aims to demonstrate a novel VF3DCP process to manufacture architectural ornaments through a case study of pattern manufacture, forgiving some manufacture errors. The mechanical functional relationships fitted through the two process tests are specifically applied for the developed VF3DCP extrusion kit prototype and the trial material; new mechanical functional relationships have to be determined if the VF3DCP machine and material are changed. However, the proposed VF3DCP method still shows an exciting possibility to construct architectural ornaments.

The VF3DCP is not just a remarkable technology but reveals a whole new way of thinking to take advantages of the 3DCP technology to make a difference to the architecture, engineering and construction community. Above all, it brings higher manufacture efficiency to the 3DCP process. Apparently, it will take much less time to manufacture a large-scale part during printing if the nozzle diameter is improved from a small value to a bigger one on the premise of required surface resolution. Since the nozzle developed in this VF3DCP extrusion kit prototype is designed up to 25mm in diameter, nozzles of larger diameter ranges as 0-100mm, 0-200mm, or even 0-1000mm can be expected as long as problems of material delivery and mechanical capability can be solved. This means an entire component can be manufactured in one-time printing work, which sharply raises productivity.

In addition, the VF3DCP method is expected to greatly enrich the product complexity and diversity. The 2.5D architectural pattern in the case study is achieved by the VF3DCP process that only changes the nozzle diameter during printing. This is accomplished within the horizontal plane, which refers to a two-dimensional volume variation dependent on the constant layer - thickness slicing condition. If a variable layer - thickness slicing algorithm is applied along with a special tool path planning algorithm, the VF3DCP process will be able to change the nozzle height when it is varying its diameter, contributing to three-dimensional volume variation printing, a genuine volume - forming fabrication process. In that context, more ornaments of complicated geometries and other components with architectural ornamentations are reachable, making the 3DCP more flexible and feasible for the future industry.

Acknowledgements

This research is supported by National Natural Science Foundation of China (No.51678265, 71732001).

Appendix A.

The fitted function is:

$$z = f(x, y) = p00 + p10*x + p01*y + p20*x^2 + p11*x*y + p02*y^2 + p30*x^3 + p21*x^2*y + p12*x*y^2 + p03*y^3 + p31*x^3*y + p22*x^2*y^2 + p13*x*y^3 + p04*y^4 + p32*x^3*y^2 + p23*x^2*y^3 + p14*x*y^4 + p05*y^5$$

$p00$ = 8.437 (4.23, 12.64)	$p10$ = -1.486 (-2.287, -0.685)
$p01$ = -0.3316 (-0.5524, -0.1109)	$p20$ = 0.08331 (0.03484, 0.1318)
$p11$ = 0.05733 (0.01865, 0.09601)	$p02$ = 0.003522 (-0.0006504, 0.007694)
$p30$ = -0.001477 (-0.002415, -0.0005378)	$p21$ = -0.002985 (-0.005233, -0.0007379)
$p12$ = -0.0003979 (-0.000873, 7.719e-05)	$p03$ = -2.895e-05 (-9.121e-05, 3.331e-05)
$p31$ = 4.934e-05 (6.834e-06, 9.185e-05)	$p22$ = 1.262e-05 (-1.107e-05, 3.631e-05)

p13 = 1.479e-06 (-8.313e-07, 3.788e-06) *p04* = 2.234e-07 (-3.267e-07, 7.735e-07)
p32 = -2.211e-08 (-4.317e-07, 3.875e-07) *p23* = -3.247e-08 (-8.037e-08, 1.543e-08)
p14 = -2.799e-09 (-1.07e-08, 5.103e-09) p05 = -7.45e-10 (-2.671e-09, 1.181e-09)
(with 95% confidence bounds)

The goodness of fit:
SSE: 0.05351; R-square: 0.9993; Adjusted R-square: 0.9987; RMSE: 0.05048

Appendix B.

The fitted function is:

*y = g (r) = p1*r^9 + p2*r^8 + p3*r^7 + p4*r^6 + p5*r^5 + p6*r^4 + p7*r^3 + p8*r^2 + p9*r + p10*

p1 = 5.805e-20 (-5.434e-20, 1.704e-19) *p2* = -1.47e-16 (-4.085e-16, 1.146e-16)
p3 = 1.596e-13 (-9.847e-14, 4.176e-13) *p4* = -9.712e-11 (-2.38e-10, 4.378e-11)
p5 = 3.629e-08 (-1.03e-08, 8.288e-08) *p6* = -8.567e-06 (-1.816e-05, 1.03e-06)
p7 = 0.001265 (4.423e-05, 0.002486) *p8* = -0.1111 (-0.2027, -0.01943)
p9 = 5.281 (1.628, 8.934) *p10* = -75.87 (-134, -17.69)
(with 95% confidence bounds)

The goodness of fit:
SSE: 0.009155; R-square: 1; Adjusted R-square: 1; RMSE: 0.09568

References

[1] B. Khoshnevis, R. Dutton, Innovative rapid prototyping process makes large sized, smooth surfaced complex shapes in a wide variety of materials, Materials Technology. 13(2) (1998) 53-56, http://dx.doi.org/10.1080/10667857.1998.11752766.
[2] S. Lim, R. A. Buswell, T. T. Le, S. A. Austin, A. G. Gibb, T. Thorpe, Developments in construction-scale additive manufacturing processes, Automation in construction. 21 (2012) 262-268, http://dx.doi.org/10.1016/j.autcon.2011.06.010.
[3] S. Lim, R. A. Buswell, P. J. Valentine et al, Modelling curved-layered printing paths for fabricating large-scale construction components, Additive Manufacturing. 12 (2016) 216-230.
[4] IAAC, Minibuilders. 2014, http://robots.iaac.net/.
[5] Rudenko, Concrete 3D Castle. 2014, http://www.totalkustom.com/.
[6] BetAbram, 2016, http://www.betabram.com/.
[7] 3dprint.com, Chinese Construction Company 3D Prints an Entire Two-Story House On-Site in 45 Days. 2016, https://3dprint.com/138664/huashang-tengda-3d-print-house/.
[8] Cnet.com, Dubai unveils world's first 3D-printed office building. 2016, https://www.cnet.com/news/dubai-unveils-worlds-first-3d-printed-office-building/.
[9] Emerging Objects, Potterbot XLS-1. 2017, http://www.emergingobjects.com/project/potterbot-xls-1/.
[10] J. Xu, L. Y. Ding, P. E. Love, Digital reproduction of historical building ornamental components: From 3D scanning to 3D printing, Automation in Construction. 76 (2017) 85-96, https://doi.org/10.1016/j.autcon.2017.01.010.
[11] N. Labonnote, A. Rønnquist, B. Manum, P. Rüther, Additive construction: State-of-the-art, challenges and opportunities, Automation in Construction. 72 (2016) 347-366, http://dx.doi.org/10.1016/j.autcon.2016.08.026.
[12] F. Bos, R. Wolfs, Z. Ahmed, T. Salet, Additive manufacturing of concrete in construction: potentials and challenges of 3D concrete printing, Virtual and Physical Prototyping. 11(3) (2016) 209-225, http://dx.doi.org/10.1080/17452759.2016.1209867.
[13] Monolite UK Ltd, 2017, http://d-shape.com/.
[14] J. Richter, The present state of accuracy in stereolithography, in: Proceedings of the Second International Conference on Rapid Prototyping, Dayton, OH, 1991, pp.269-294.
[15] J. G. Zhou, D. Herscovici, C. C. Chen, Parametric process optimization to improve the accuracy of rapid prototyped stereolithography parts, International Journal of Machine Tools and Manufacture. 40(3) (2000) 363-379.
[16] H. Wenbin, L. Yong Tsui, G. Haiqing, A study of the staircase effect induced by material shrinkage in rapid prototyping, Rapid Prototyping Journal. 11(2) (2005) 82-89.
[17] T. T. Le, S. A. Austin, S. Lim, R. A. Buswell, A. G. Gibb, T. Thorpe, Mix design and fresh properties for high-performance printing concrete, Materials and structures. 45(8) (2012) 1221-1232.
[18] J. W. Brandt, V. R. Algazi, Continuous skeleton computation by Voronoi diagram, CVGIP: Image understanding. 55(3) (1992) 329-338.
[19] R. Duballet, O. Baverel & J. Dirrenberger, Classification of building systems for concrete 3D printing, Automation in Construction. 83 (2017) 247-258.